# Importance of Diameter Control on Selective Synthesis of Semiconducting Single-Walled Carbon Nanotubes

Jinghua Li,[†] Chung-Ting Ke,[‡] Kaihui Liu,[§] Pan Li,[†] Sihang Liang,[§] Gleb Finkelstein,[‡] Feng Wang,[§] and Jie Liu[†,*]

[†]Department of Chemistry and [‡]Department of Physics, Duke University, Durham, North Carolina 27708, United States, and [§]Department of Physics, University of California at Berkeley, Berkeley, California 94720, United States

ABSTRACT The coexistence of semiconducting and metallic single-walled carbon nanotubes (SWNTs) during synthesis is one of the major bottlenecks that prevent their broad application for the next-generation nanoelectronics. Herein, we present more understanding and demonstration of the growth of highly enriched semiconducting SWNTs (s-SWNTs) with a narrow diameter distribution. An important fact discovered in our experiments is that the

selective elimination of metallic SWNTs (m-SWNTs) from the mixed arrays grown on quartz is diameter-dependent. Our method emphasizes controlling the diameter distribution of SWNTs in a narrow range where m-SWNTs can be effectively and selectively etched during growth. In order to achieve narrow diameter distribution, uniform and stable Fe–W nanoclusters were used as the catalyst precursors. About 90% of as-prepared SWNTs fall into the diameter range 2.0–3.2 nm. Electrical measurement results on individual SWNTs confirm that the selectivity of s-SWNTs is ∼95%. The present study provides an effective strategy for increasing the purity of s-SWNTs *via* controlling the diameter distribution of SWNTs and adjusting the etchant concentration. Furthermore, by carefully comparing the chirality distributions of Fe–W-catalyzed and Fe-catalyzed SWNTs under different water vapor concentrations, the relationship between the diameter-dependent and electronic-type-dependent etching mechanisms was investigated.
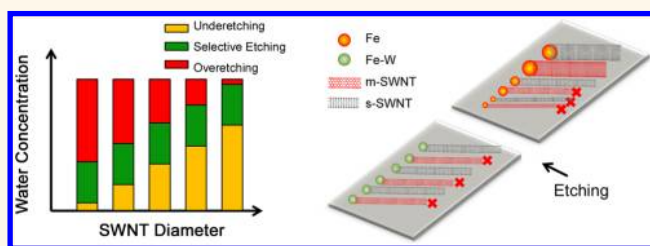
KEYWORDS: single-walled carbon nanotubes · semiconducting · diameter control · selective etching · Fe–W nanoclusters

Carbon nanotubes (CNTs), especially single-walled carbon nanotubes (SWNTs), are promising candidates for the development of electronic devices beyond silicon because of the unique structure and outstanding properties.[1–13] SWNTs can be either semiconducting or metallic, denoted as s- and m-SWNTs, respectively. Particularly, s-SWNTs can be used as the channels in field-effect transistors (FETs). However, a major bottleneck for the broad application of SWNTs is the coexistence of s- and m-SWNTs in as-synthesized samples, the latter of which can cause low on/off ratios in FETs. Therefore, obtaining pure s-SWNTs is a significant challenge for the research field.

Over the past decade, great progress has been made trying to solve this problem. Many research groups developed various separation methods to obtain either pure s-SWNTs or pure m-SWNTs.[10,14–18] However, these approaches often result in short tube length, high defect density, or contaminations of SWNTs, which may affect the performance of nanotube-based devices. As an alternative, the chemical vapor deposition (CVD) method has been proven to be a reliable and effective way to directly synthesize s-SWNTs with high quality on target substrates. Previously, both theoretical and experimental studies showed that m-SWNTs are more reactive than s-SWNTs due to the lower ionization energy.[19–21] Accordingly, different strategies have been developed to selectively eliminate m-SWNTs from the as-prepared nanotubes with mixed electronic structures made by the CVD method, including using etchants such as methanol,[22] oxygen,[23] water,[24,25] and hydrogen,[26] applying isopropyl alcohol as the –OH-containing carbon feedstock,[27] introducing UV light during growth,[28] or choosing oxidative catalyst supports.[29] However, some recent studies reported that the etching of SWNTs is not only electronic-type-dependent but also diameter-dependent.[30,31] Particularly, our group discovered that there is a very narrow "optimal range" of SWNT

diameter under certain etching conditions where most m-SWNTs are eliminated while s-SWNTs survive, and for SWNTs with diameters out of the "optimal range", no obvious selectivity is observed.[32] These facts indicate that the electronic-type-dependent and diameter-dependent etching mechanisms may entangle together during growth, which makes the selective synthesis of s-SWNTs more complex since both mechanisms should be taken into consideration.

In this study, an effective approach was developed to successfully synthesize highly selective s-SWNTs with a narrow diameter distribution. It has been suggested that there is a positive correlation between the diameters of SWNTs and the size of the catalyst particles.[33−36] Therefore, a possible way for controlling the diameter of SWNTs is to select a catalyst that can be uniformly dispersed on the substrate surface. In our typical CVD growth method, iron is used as the catalyst because of its high nucleation activity. However, Fe nanoparticles have a relatively low melting point among metals and could be in the liquid state with considerable mobility under high temperature during CVD growth (900 °C),[37] which results in a broad distribution of the catalyst particle size according to the Ostwald ripening mechanism.[38] Recently, it was reported that tungsten-containing nanoclusters are not only uniform in size but also stable during CVD synthesis due to the high-temperature stability of W.[39] Thus, in the present work, an Fe−W nanocluster was chosen as the catalyst precursor to obtain diameter-controlled

SWNTs on the quartz substrate. It is discovered that by applying water vapor as the etchant to the growth environment, the selectivity of s-SWNTs reaches up to ~95% on quartz based on results from electrical measurement and *in situ* optical spectroscopy on individual nanotubes.[40] By comparing the selectivity of Fe−W-catalyzed and Fe-catalyzed SWNTs grown under different etching conditions, the relationship between the electronic-type-dependent and diameter-dependent etching mechanisms was revealed.

RESULTS AND DISCUSSION

In order to obtain information on the size distribution of the catalyst particles, the molecular nanoclusters $Na_{16}K_{12}[H_{56}P_8W_{48}Fe_{28}O_{248}] \cdot 90H_2O$ (denoted as Fe−W clusters) were synthesized and dispersed on a SiO_2/Si substrate (see Methods section for details). The clusters were annealed in the air and then reduced in hydrogen. For comparison, an $FeCl_3$ solution was also prepared and treated under the same condition to form Fe nanoparticles. A typical CVD growth procedure of 15 min was performed using both catalyst precursors. Afterward, areas between nanotubes were imaged by atomic force microscopy (AFM). The reason for treating the nanoparticles under the same CVD growth conditions is to confirm whether the Fe−W nanoparticles have a more uniform size distribution during and after the high-temperature process (including both the catalyst reduction and growth steps). Figure 1 shows the AFM images and size
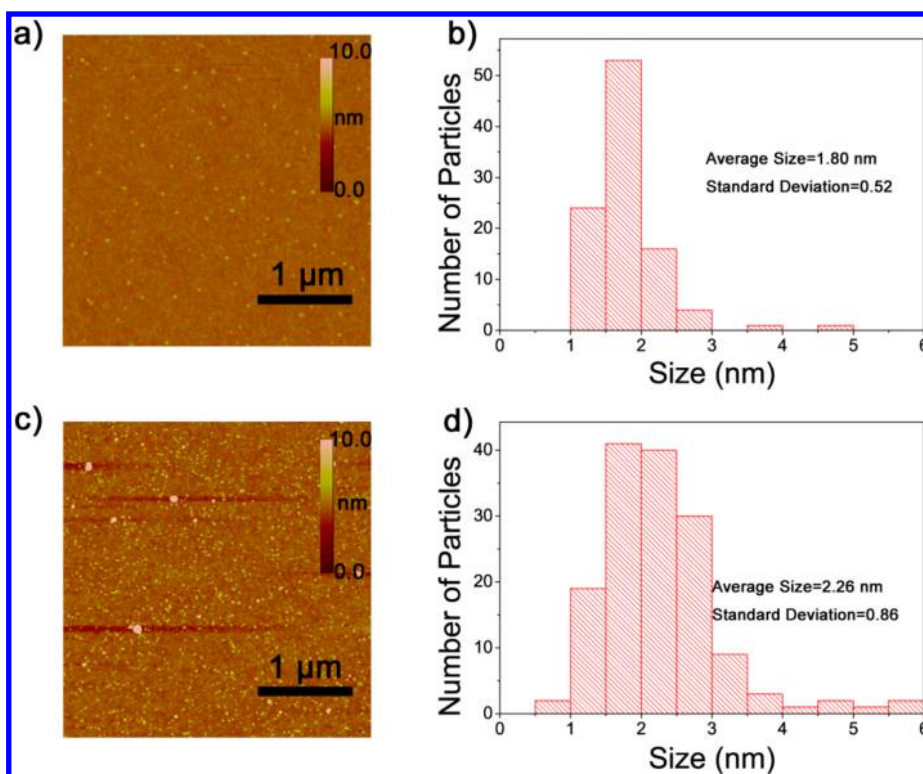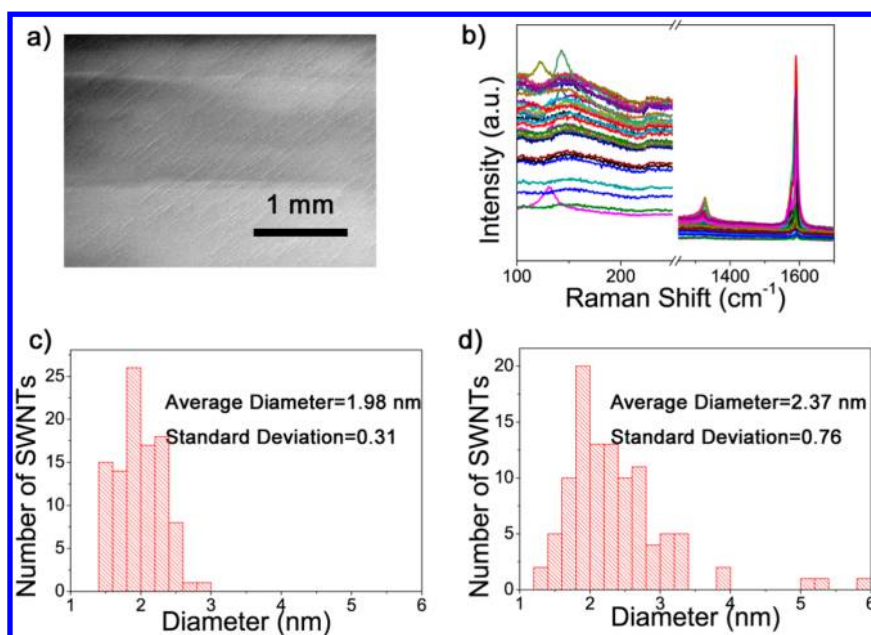

Figure 1. AFM images for Fe−W (a) and Fe (c) nanoparticles on the SiO_2/Si substrate. Size distributions for Fe−W (b) and Fe (d) nanoparticles after CVD growth for 15 min at 900 °C. Over 100 particles were measured for each sample.

Figure 2. (a) SEM image of Fe−W-catalyzed SWNTs synthesized on a quartz substrate with a water vapor concentration of 522 ppm. (b) Raman spectra of Fe−W-catalyzed SWNTs showing RBM peaks, D bands, and G bands under an excitation laser of 633 nm. (c, d) Diameter distributions of Fe−W-catalyzed SWNTs (c) and Fe-catalyzed SWNTs (d) measured by AFM.

distributions of the Fe−W (a, b) and Fe (c, d) nanoparticles, respectively. Clearly, Fe−W nanoparticles are more uniformly distributed on the substrate surface. It should be noted that in Figure 1 the Fe−W catalyst nanoparticles are sparse on the substrate compared with Fe nanoparticles. To clarify the effect of the catalyst precursor concentration on the particle size distribution, we performed another group of experiments, where the FeCl$_3$ solution was diluted to 1/10 of the original concentration and then spin-coated onto the substrate. As shown in Figure S1, both the average size and standard deviation of as-prepared Fe nanoparticles slightly decreased compared with those from the undiluted solution. However, these values are still larger than those of Fe−W nanoparticles, and some aggregations can be observed. This fact indicates that even though the concentration is playing a role, the intrinsic property of the catalyst nanoparticles is a crucial factor determining their size distribution. Because of its size uniformity and high-temperature stability, the Fe−W nanocluster is considered to be a better catalyst precursor to obtain SWNTs with a narrow diameter distribution.

Figure 2a shows the scanning electron microscopy (SEM) image of the horizontally aligned SWNTs synthesized on a 36° Y-cut quartz substrate using Fe−W nanoparticles. The SEM images at a higher magnification of both Fe−W-catalyzed and Fe-catalyzed SWNTs are shown in Figure S2. Interestingly, it is found that Fe−W catalysts tend to nucleate shorter SWNTs with lower density. The observation could be understood by considering the relatively slower SWNT nucleation speed on the Fe−W catalyst than on the Fe catalyst

due to the decrease of the active Fe component. Both Fe−W-catalyzed and Fe-catalyzed SWNTs show some hook-shaped structures (the latter is clear only when zoomed in), which are found to be a common phenomenon for SWNTs nucleated by spin-coated catalysts.[41] For Raman characterization and device fabrication, the as-prepared SWNTs were transferred from quartz to a SiO$_2$/Si substrate by using the previously reported polymer-assisted method.[22] The low D/G ratios under the excitation laser of 633 nm for Raman spectroscopy confirm the existence of SWNTs (Figure 2b). Note that not all nanotubes show radial breathing mode (RBM) peaks. According to the Kataura plot, under 633 nm laser excitation the expected Raman shift frequency (ω) ranges from 120 to 170 cm^{-1} for s-SWNTs and from 180 to 230 cm^{-1} for m-SWNTs. On the basis of the experimental relationship $\omega = 248/d$ (d is the diameter in nm), s-SWNTs and m-SWNTs that can be detected are estimated to be within the diameter ranges 1.5−2.1 and 1.1−1.4 nm. The result indicates that the diameters of some nanotubes are out of the ranges mentioned above, leading to fewer RBM peaks in Figure 2b. As determined by AFM, the Fe−W-catalyzed SWNTs show a narrower diameter distribution (Figure 2c) compared to Fe-catalyzed SWNTs (Figure 2d). The AFM images for Fe−W-catalyzed SWNTs and Fe-catalyzed SWNTs are shown in Figure S3. The average diameter of as-prepared SWNTs is larger than the previously reported average diameter of tubes grown on quartz, which is normally 1.2−1.6 nm, and the observation can be attributed to two possible reasons: on one hand, the present Fe−W catalyst favors the nucleation of SWNTs with larger
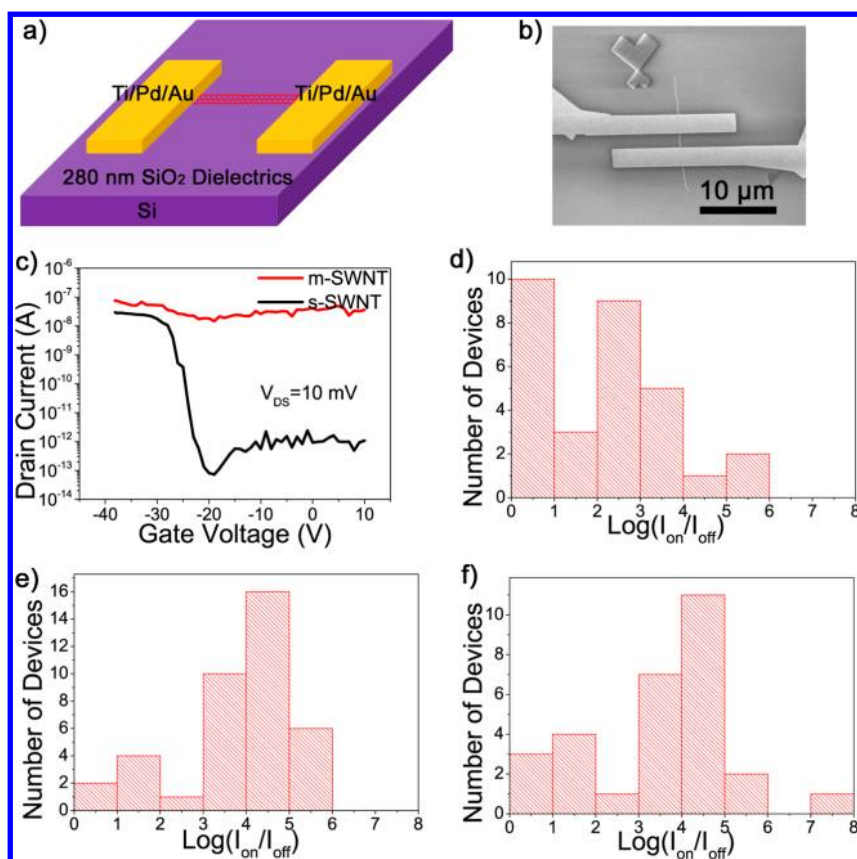
Figure 3. (a) Schematic illustration of an individual tube FET device. (b) SEM image of an individual tube device with a channel length of 2 μm. (c) Transfer characteristics of a semiconducting SWNT (black line) and a metallic SWNT (red line). (d−f) Histograms of the on/off ratio of each individual tube device based on Fe−W-catalyzed SWNTs synthesized without water vapor (d), with a water vapor concentration of 1036 ppm during growth (e), and with a water vapor concentration of 594 ppm after growth (f).

diameter, and on the other hand, smaller diameter SWNTs are generally more reactive because of the strain and thus are more easily eliminated from the mixed array.

Electrical measurements of FETs based on individual SWNTs were performed to evaluate the selectivity of as-synthesized SWNTs. In a typical process, the fabrication of FETs was conducted on SiO$_2$/Si substrates with 280 nm SiO$_2$ dielectrics. The channel length was 2 μm (see Method section for details). Highly doped Si was used as the back gate, and the source−drain voltage was 10 mV. Figure 3a and b show the schematic illustration and SEM image of a representative device. The electron transfer characteristics of an m-SWNT (red line) and an s-SWNT (black line) are provided in Figure 3c. The statistics of on/off ratios of Fe−W-catalyzed SWNTs synthesized without water vapor are shown in Figure 3d. Out of the 30 devices, 10 transistors were found to have on/off ratios lower than 10, which indicates the metallic properties of the corresponding SWNTs. Considering the fact that m-SWNTs should account for 1/3 of all the tubes if the nanotubes with each chirality have equal opportunities to grow during CVD synthesis, using only Fe−W catalysts does not obviously result in selective enrichment of s-SWNTs.

When an appropriate amount of water vapor was introduced into the CVD system during synthesis, a significant increase in the selectivity was observed. Figure 3e shows the statistics of the on/off ratios of devices based on SWNTs synthesized under the same growth condition as in Figure 3d except the addition of water vapor with a concentration of 1036 ppm during synthesis. The statistics of the on-state current of each device are shown in Figure S4 to demonstrate that the devices are of good performance. Two SWNTs with an on/off ratio lower than 10 were identified out of 39 randomly selected nanotubes. On the basis of this result, the ratio of s-SWNTs is roughly estimated to be ∼95%. To have a more complete understanding, different etching conditions were tested on the Fe−W-catalyzed SWNTs, and it was found that high selectivity can be reproducibly obtained either by *in situ* or postsynthesis water vapor treatment. For instance, it is shown in Figure 3f that the ratio of s-SWNTs is ∼90% for Fe−W-catalyzed SWNTs treated with water vapor (concentration = 594 ppm) for 20 min after CVD growth. It was also noticed that an excessive amount of etchant will cause a decrease in the selectivity. As shown in Figure S5, when the water vapor concentration during CVD growth was increased to 2629 ppm,
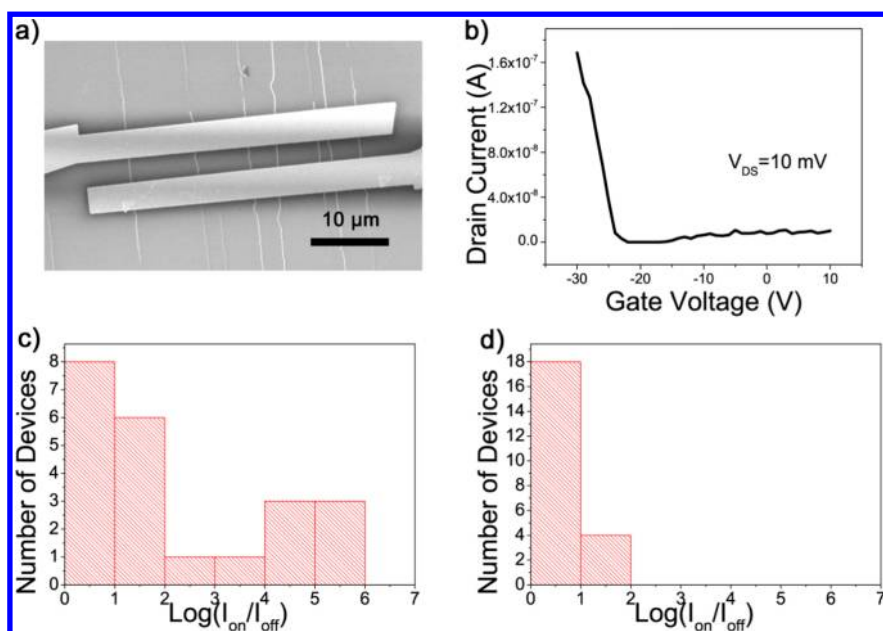
Figure 4. (a) SEM image of a multiple-tube device with a channel length of 2 μm. (b) Transfer characteristics of a representative multiple-tube device. (c, d) Histograms of the on/off ratio of each multiple-tube device based on Fe−W-catalyzed (c) and Fe-catalyzed (d) SWNTs under optimized water vapor concentration during growth.

the ratio of s-SWNTs dropped to ∼70%. This is consistent with the result in our previous publication.[25] A possible explanation for such an observation is that both m- and s-SWNTs can be oxidized under high water vapor concentrations, and consequently, the etching is no longer selective toward the electronic structures of SWNTs.

The other important factor identified in achieving high selectivity growth of s-SWNTs is the narrow diameter distribution. To demonstrate the diameter-dependent effect, Fe−W-catalyzed SWNTs were compared to Fe-catalyzed SWNTs using the electrical measurement of an FET device containing 2−12 nanotubes (see Figure 4a). Figure 4b shows the electron transfer characteristics of a representative device based on Fe−W-catalyzed SWNTs, and the on/off ratio is ∼80 000. For Fe−W-catalyzed SWNTs synthesized with water vapor concentration of 1036 ppm, ∼68% devices showed an on/off ratio larger than 10 (Figures 4c, S6a). In contrast, for Fe-catalyzed SWNTs with water vapor etching, only four devices out of 22 (∼18%) were identified to have an on/off ratio above 10, indicating that the diameter-controlled SWNTs have better selectivity under the optimized growth conditions (see Figure 4d and Figure S6b).

The newly developed polarization-based optical spectroscopy combined with a supercontinuum laser light source was also used to further demonstrate the diameter and chirality distributions of individual Fe−W-catalyzed SWNTs.[40] This method has been proven to offer fast and accurate characterization of the chirality of SWNTs. Figure S7 shows the optical spectra of a (21,11) SWNT (a, semiconducting) and a (25,13) SWNT (b, metallic). The optical spectroscopy further

confirms that all the as-prepared nanotubes are singewalled because multiwalled carbon nanotubes (MWNTs) often show coupled spectral features, i.e., more resonant peaks and higher optical signal, which were not detected in our samples. For each sample, the (n,m) values of over 50 SWNTs were determined by optical spectroscopy, and the diameters were calculated accordingly. Figure 5a shows the diameter and chirality distributions of Fe−W-catalyzed SWNTs synthesized with a water vapor concentration of 522 ppm. The detailed statistics of the (n,m) values are shown in Table S1 in the Supporting Information. The ratio of as-prepared SWNTs that fall into the diameter range from 2.0 to 3.2 nm is ∼90%. It should be noted that the calculated average diameter is larger than that measured by AFM, and that could be understood by considering that the interaction between SWNTs and the substrate/AFM tip might cause the deformation of the tubes, which is consistent with our earlier study.[22] More Fe−W-catalyzed SWNTs under different etching conditions were characterized, and it was identified that with a water vapor concentration between 522 and 1036 ppm s-SWNTs account for 81−85% of all the measured tubes. These ratios are lower than the value of 95% determined by the electrical measurement on individual SWNTs (water vapor concentration = 1036 ppm). The difference can be explained as follows: the "semimetallic" SWNTs ($n − m = 3i$, and i is an integer) having small band gaps may show an on/off ratio larger than 10.[42] In fact, according to Table S1, only one tube out of 52 has the armchair structure ($n = m$), and the semiconducting and semimetallic SWNTs account for ∼98% of all the tubes. For comparison, the chiralities of Fe-catalyzed SWNTs with water vapor etching during
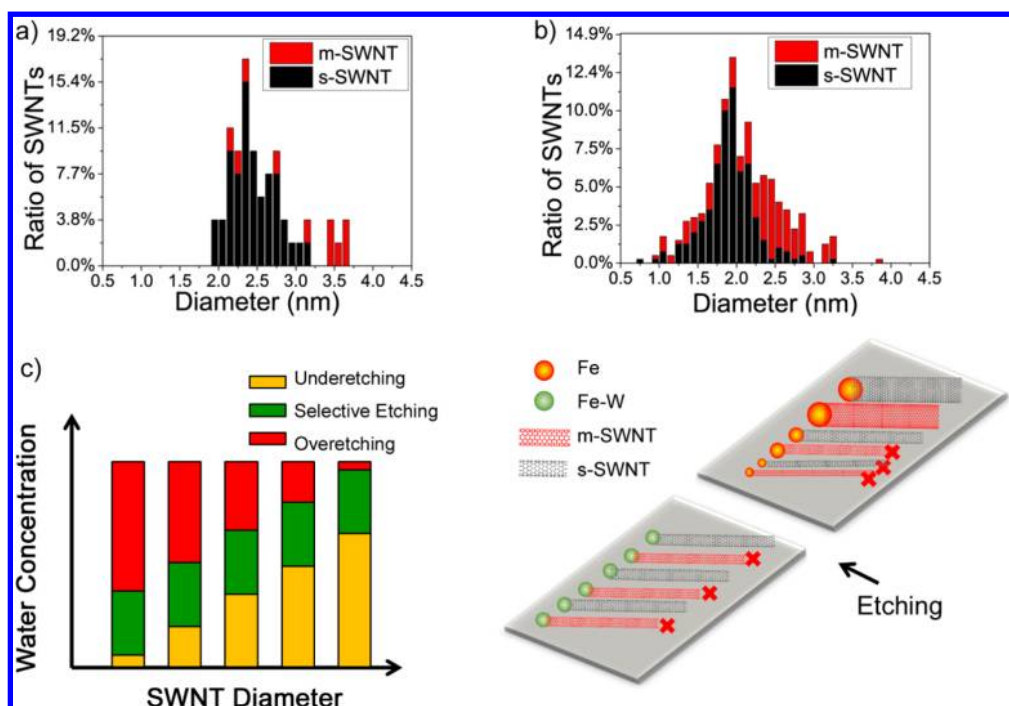
Figure 5. (a) Diameter and chirality distributions of the Fe—W-catalyzed SWNTs under a water vapor concentration of 522 ppm. (b) Diameter and chirality distributions of the Fe-catalyzed SWNTs under a water vapor concentration of 496 ppm. (c) Schematic illustration of the diameter-dependent and electronic-type-dependent etching mechanisms.

growth (496 ppm) were also mapped out. A much broader diameter distribution was observed, as shown in Figure 5b (this figure was modified from our previous publications).[32,40] The diameter range for the best selectivity is found to be approximately from 1.2 to 2.2 nm, where ~80% tubes are categorized to be s-SWNTs based on the (n,m) values. However, the growth and etching conditions do not demonstrate a selective effect for SWNTs out of this range, resulting in the low overall s-SWNT percentage. Interestingly, it was also noticed that the "best selective ranges" of the diameters for the Fe—W-catalyzed and Fe-catalyzed SWNTs mentioned above are different under the water vapor etching conditions around 500 ppm. This fact implies that the catalysts could have more functions, such as predetermining the structures of nucleated nanotubes or affecting the etching reaction, than just controlling the diameter of SWNTs. Details on the roles of catalysts are worth further study and have already been under way in our group.

To better elucidate the correlation between the diameter-dependent and electronic-type-dependent etching mechanisms, the chirality and diameter distributions of Fe-catalyzed SWNTs synthesized under different growth conditions were also carefully investigated. Figure S8 shows the diameter and chirality distributions of SWNTs synthesized without water vapor (a) and with a considerable amount of water vapor (2541 ppm) (b) (Figure S8a was modified from our previous publication).[32] It is shown in Figure S8a

that Fe-catalyzed SWNTs synthesized without water vapor do not have any overall selectivity, which is similar to the electrical measurement result on the corresponding Fe—W-catalyzed SWNTs. Nevertheless, it was found that as-prepared SWNTs with a diameter smaller than 1.4 nm are all semiconducting. A possible reason for such a fact is that the carbon feedstock, ethanol, contains the —OH group and can act as a weak etchant. It was reported that small-diameter SWNTs are more reactive than large-diameter counterparts because of the higher curvature.[30,43,44] Therefore, small-diameter m-SWNTs were the first to be removed under this growth condition. When the water vapor concentration was increased to 2541 ppm, SWNTs with a diameter smaller than 2.8 nm show no selectivity. However, all m-SWNTs with a diameter larger than 2.8 nm disappear, and the only two SWNTs detected are semiconducting. The difficulty in finding more s-SWNTs is due to the fact that for the diameter range larger than ~3.0 nm m-SWNTs seem to have a higher chance of being nucleated, as clearly shown in Figures 5a,b and S8a, and this observation also implies that if the diameter of most SWNTs could be tuned to larger than 3.0 nm, high selectivity for m-SWNTs could be achieved. This set of data indicates that the diameter range within which selectivity was observed tends to upshift as the water vapor concentration increases. Figure S9 summarizes the selective etching window for Fe-catalyzed SWNTs under different water vapor concentrations, in agreement with this conclusion.

Thus, the relationship between the diameter-dependent and electronic-type-dependent etching mechanisms can be summarized as follows: (i) For SWNTs with a predefined diameter, there is a "selective etching window" of the water vapor concentration under which high selectivity can be achieved. The water vapor concentrations below the range are not strong enough to totally eliminate the m-SWNTs (underetching), and the ones above this range might oxidize SWNTs with both electronic structures, which makes the etching reaction no longer selective (overetching). (ii) The "selective etching window" is diameter-dependent due to the difference in strains. In the meantime, it should also be pointed out that the proposed rules do not necessarily apply to carbon nanotubes with a high defect density, such as MWNTs, where the etching reaction might be mainly defect-dependent. The schematic illustration for the as-stated mechanisms is summarized in Figure 5c. As a result, for SWNTs with a broad diameter distribution, selective etching was observed only within a narrow diameter range under a certain growth condition. By controlling the diameter using the Fe–W catalysts, an effective etching concentration window can be identified to obtain a high selectivity of s-SWNTs.

CONCLUSION

In conclusion, horizontally aligned s-SWNTs with a high selectivity were successfully obtained on a Y-cut quartz substrate by the strategy of combining diameter control and electronic-type-selective etching. Statistics on electrical measurement of individual SWNTs show that the selectivity can reach up to ~95%. The comparison between the performances of FETs based on Fe–W-catalyzed and Fe-catalyzed SWNTs verified that the diameter control is a critical factor in obtaining highly selective s-SWNTs. The newly developed optical imaging technique further confirms that the as-prepared SWNTs are of high selectivity and uniform diameter when Fe–W catalysts are used. In addition, the relationship between the diameter-dependent and electronic-type-dependent etching mechanisms was proposed by systematically exploring the diameter and chirality distributions of Fe–W-catalyzed and Fe-catalyzed SWNTs under different etching conditions. Although detailed mechanisms on the etching reaction might vary due to different catalysts, substrates, and carbon feedstocks, we believe that this method could potentially become a general approach to obtain s-SWNTs with high purity.

METHODS

Preparation of Nanocluster Catalyst Precursors. The Fe–W nanoclusters were synthesized according to previous literature.[45,46] A 15 mg amount of polystyrene-*b*-poly(2-vinylpyridine) was dispersed in 15 mL of toluene to form micelles, and ~1 mg of nanoclusters was subsequently added. The suspension was vigorously stirred for 7 days and spin-coated onto the substrate for CNT growth. For the control group, ~1 mg of FeCl$_3$ was used with other conditions being the same.

Growth of Horizontally Aligned SWNTs on the Quartz Substrate. The quartz substrates with catalyst precursors were annealed in the air at 775 °C in a 1 in. Linderberg furnace for 30 min to remove polymers before cooling to room temperature. Then the furnace was heated to 775 °C, and the catalyst precursors were reduced under a H$_2$ flow at 367 sccm for 15 min. For a typical CVD growth process, a H$_2$ flow at 279 sccm, an Ar flow at 70 sccm through an ethanol bubbler, and another Ar flow at varied rates (0, 30, 65, and 231 sccm) through a water bubbler were introduced to the system. The bubblers were kept in a mixture of ice and water to maintain a constant temperature around 0 °C. The growth lasted for 15 min at 900 °C. The system was cooled to room temperature with the protection of H$_2$.

Characterization. A scanning electron microscope (FEI XL30 S-FEG, operated at 1.5 kV), an atomic force microscope (Digital Instruments Multiple Mode SPM Nanoscope IIIa, operated at tapping-mode), and a micro-Raman spectroscope (Horiba Jobin Yvon LabRam ARAMIS) were used for the characterization of SWNTs synthesized. The wavelength of the excitation laser for Raman spectroscopy was 633 nm. The optical imaging and spectroscopy for the chirality distribution of SWNTs followed the previously stated approach.[40]

Fabrication and Measurement of Back-Gate Field-Effect Transistors. The SWNTs on quartz were transferred from quartz to a SiO$_2$/Si substrate with a 280 nm oxide layer by using the previously reported polymer-assisted method.[22] Electrodes were patterned by e-beam lithography with a channel length of 2 μm. Ti (1.2 nm)/Pd (20 nm)/Au (40 nm) were deposited by e-beam evaporation. Another lithography step was taken to remove SWNTs outside the channel by oxygen plasma. The electrical measurement was performed by a Keithley 4200-SCS semiconductor characterization system. The gate voltage was 10 mV.

Conflict of Interest: The authors declare no competing financial interest.

Supporting Information Available: AFM image and size distribution of Fe nanoparticles with a diluted density (~1/10), additional SEM and AFM images of Fe–W- and Fe-catalyzed SWNTs synthesized on quartz substrates, statistics of the on-state current of devices based on individual Fe–W-catalyzed SWNTs (water vapor concentration = 1036 ppm), histograms of the on/off ratio of each individual tube device based on Fe–W-catalyzed SWNTs (water vapor concentration = 2629 ppm), displays of on/off ratio of multiple-tube devices based on Fe–W- and Fe-catalyzed SWNTs under the optimized etching conditions, optical spectra of a (21,11) s-SWNT and a (25,13) m-SWNT, chirality and diameter distributions of Fe-catalyzed SWNTs synthesized with water vapor concentrations of 0 and 2541 ppm, selective etching windows of Fe-catalyzed SWNTs under different water vapor concentrations, chiralities of Fe–W-catalyzed SWNTs synthesized with a water vapor concentration of 522 ppm. This material is available free of charge *via* the Internet at http://pubs.acs.org.

REFERENCES AND NOTES

1. Bockrath, M.; Cobden, D. H.; McEuen, P. L.; Chopra, N. G.; Zettl, A.; Thess, A.; Smalley, R. E. Single-Electron Transport in Ropes of Carbon Nanotubes. *Science* **1997**, *275*, 1922–1925.

2. Chen, Z.; Appenzeller, J.; Lin, Y. M.; Sippel-Oakley, J.; Rinzler, A. G.; Tang, J.; Wind, S. J.; Solomon, P. M.; Avouris, P. An Integrated Logic Circuit Assembled on a Single Carbon Nanotube. *Science* **2006**, *311*, 1735–1735.

3. Dresselhaus, M. S.; Dresselhaus, G.; Eklund, P. C. In *Science of Fullerenes and Carbon Nanotubes: Their Properties and Applications*; Academic Press: San Diego, 1996.

4. Iijima, S.; Ichihashi, T. Single-Shell Carbon Nanotubes of 1-nm Diameter. *Nature* **1993**, *363*, 603–605.

5. Javey, A.; Guo, J.; Wang, Q.; Lundstrom, M.; Dai, H. J. Ballistic Carbon Nanotube Field-Effect Transistors. *Nature* **2003**, *424*, 654–657.

6. Javey, A.; Kim, H. S.; Brink, M.; Wang, Q.; Ural, A.; Guo, J.; McIntyre, P.; McEuen, P.; Lundstrom, M.; Dai, H. J. High-κ Dielectrics for Advanced Carbon-Nanotube Transistors and Logic Gates. *Nat. Mater.* **2002**, *1*, 241–246.

7. Pop, E.; Mann, D.; Wang, Q.; Goodson, K.; Dai, H. J. Thermal Conductance of an Individual Single-Wall Carbon Nanotube above Room Temperature. *Nano Lett.* **2006**, *6*, 96–100.

8. Saito, R.; Dresselhaus, G.; Dresselhaus, M. S. In *Physical Properties of Carbon Nanotubes*; Imperial College Press: London, 1998.

9. Tans, S. J.; Devoret, M. H.; Dai, H. J.; Thess, A.; Smalley, R. E.; Geerligs, L. J.; Dekker, C. Individual Single-Wall Carbon Nanotubes as Quantum Wires. *Nature* **1997**, *386*, 474–477.

10. Wang, C.; Zhang, J.; Ryu, K.; Badmaev, A.; De Arco, L. G.; Zhou, C. Wafer-Scale Fabrication of Separated Carbon Nanotube Thin-Film Transistors for Display Applications. *Nano Lett.* **2009**, *9*, 4285–4291.

11. Tans, S. J.; Verschueren, A. R. M.; Dekker, C. Room-Temperature Transistor Based on a Single Carbon Nanotube. *Nature* **1998**, *393*, 49–52.

12. Kang, S. J.; Kocabas, C.; Ozel, T.; Shim, M.; Pimparkar, N.; Alam, M. A.; Rotkin, S. V.; Rogers, J. A. High-Performance Electronics Using Dense, Perfectly Aligned Arrays of Single-Walled Carbon Nanotubes. *Nat. Nanotechnol.* **2007**, *2*, 230–236.

13. Sun, D. M.; Timmermans, M. Y.; Tian, Y.; Nasibulin, A. G.; Kauppinen, E. I.; Kishimoto, S.; Mizutani, T.; Ohno, Y. Flexible High-Performance Carbon Nanotube Integrated Circuits. *Nat. Nanotechnol.* **2011**, *6*, 156–161.

14. LeMieux, M. C.; Sok, S.; Roberts, M. E.; Opatkiewicz, J. P.; Liu, D.; Barman, S. N.; Patil, N.; Mitra, S.; Bao, Z. Solution Assembly of Organized Carbon Nanotube Networks for Thin-Film Transistors. *ACS Nano* **2009**, *3*, 4089–4097.

15. Engel, M.; Small, J. P.; Steiner, M.; Freitag, M.; Green, A. A.; Hersam, M. C.; Avouris, P. Thin Film Nanotube Transistors Based on Self-Assembled, Aligned, Semiconducting Carbon Nanotube Arrays. *ACS Nano* **2008**, *2*, 2445–2452.

16. Park, H.; Afzali, A.; Han, S. J.; Tulevski, G. S.; Franklin, A. D.; Tersoff, J.; Hannon, J. B.; Haensch, W. High-Density Integration of Carbon Nanotubes *via* Chemical Self-Assembly. *Nat. Nanotechnol.* **2012**, *7*, 787–791.

17. Lee, H. W.; Yoon, Y.; Park, S.; Oh, J. H.; Hong, S.; Liyanage, L. S.; Wang, H. L.; Morishita, S.; Patil, N.; Park, Y. J.; *et al*. Selective Dispersion of High Purity Semiconducting Single-Walled Carbon Nanotubes with Regioregular Poly(3-alkylthiophene)s. *Nat. Commun.* **2011**, *2*, 541.

18. Tanaka, T.; Liu, H. P.; Fujii, S.; Kataura, H. From Metal/Semiconductor Separation to Single-Chirality Separation of Single-Wall Carbon Nanotubes Using Gel. *Phys. Status Solidi RRL* **2011**, *5*, 301–306.

19. Strano, M. S.; Dyke, C. A.; Usrey, M. L.; Barone, P. W.; Allen, M. J.; Shan, H. W.; Kittrell, C.; Hauge, R. H.; Tour, J. M.; Smalley, R. E. Electronic Structure Control of Single-Walled Carbon Nanotube Functionalization. *Science* **2003**, *301*, 1519–1522.

20. Lu, J.; Nagase, S.; Zhang, X. W.; Wang, D.; Ni, M.; Maeda, Y.; Wakahara, T.; Nakahodo, T.; Tsuchiya, T.; Akasaka, T.; *et al*. Selective Interaction of Large or Charge-Transfer Aromatic Molecules with Metallic Single-Wall Carbon Nanotubes: Critical Role of the Molecular Size and Orientation. *J. Am. Chem. Soc.* **2006**, *128*, 5114–5118.

21. An, L.; Fu, Q. A.; Lu, C. G.; Liu, J. A Simple Chemical Route to Selectively Eliminate Metallic Carbon Nanotubes in Nanotube Network Devices. *J. Am. Chem. Soc.* **2004**, *126*, 10520–10521.

22. Ding, L.; Tselev, A.; Wang, J.; Yuan, D.; Chu, H.; McNicholas, T. P.; Li, Y.; Liu, J. Selective Growth of Well-Aligned Semiconducting Single-Walled Carbon Nanotubes. *Nano Lett.* **2009**, *9*, 800–805.

23. Yu, B.; Liu, C.; Hou, P. X.; Tian, Y.; Li, S. S.; Liu, B. L.; Li, F.; Kauppinen, E. I.; Cheng, H. M. Bulk Synthesis of Large Diameter Semiconducting Single-Walled Carbon Nanotubes by Oxygen-Assisted Floating Catalyst Chemical Vapor Deposition. *J. Am. Chem. Soc.* **2011**, *133*, 5232–5235.

24. Li, P.; Zhang, J. Sorting out Semiconducting Single-Walled Carbon Nanotube Arrays by Preferential Destruction of Metallic Tubes Using Water. *J. Mater. Chem.* **2011**, *21*, 11815–11821.

25. Zhou, W.; Zhan, S.; Ding, L.; Liu, J. General Rules for Selective Growth of Enriched Semiconducting Single Walled Carbon Nanotubes with Water Vapor as *in Situ* Etchant. *J. Am. Chem. Soc.* **2012**, *134*, 14019–14026.

26. Li, W. S.; Hou, P. X.; Liu, C.; Sun, D. M.; Yuan, J. T.; Zhao, S. Y.; Yin, L. C.; Cong, H. T.; Cheng, H. M. High-Quality, Highly Concentrated Semiconducting Single-Wall Carbon Nanotubes for Use in Field Effect Transistors and Biosensors. *ACS Nano* **2013**, *7*, 6831–6839.

27. Che, Y. C.; Wang, C.; Liu, J.; Liu, B. L.; Lin, X.; Parker, J.; Beasley, C.; Wong, H. S. P.; Zhou, C. W. Selective Synthesis and Device Applications of Semiconducting Single-Walled Carbon Nanotubes Using Isopropyl Alcohol as Feedstock. *ACS Nano* **2012**, *6*, 7454–7462.

28. Hong, G.; Zhang, B.; Peng, B.; Zhang, J.; Choi, W. M.; Choi, J. Y.; Kim, J. M.; Liu, Z. Direct Growth of Semiconducting Single-Walled Carbon Nanotube Array. *J. Am. Chem. Soc.* **2009**, *131*, 14642–14643.

29. Qin, X. J.; Peng, F.; Yang, F.; He, X. H.; Huang, H. X.; Luo, D.; Yang, J.; Wang, S.; Liu, H. C.; Peng, L. M.; *et al*. Growth of Semiconducting Single-Walled Carbon Nanotubes by Using Ceria as Catalyst Supports. *Nano Lett.* **2014**, *14*, 512–517.

30. Zhang, G. Y.; Qi, P. F.; Wang, X. R.; Lu, Y. R.; Li, X. L.; Tu, R.; Bangsaruntip, S.; Mann, D.; Zhang, L.; Dai, H. J. Selective Etching of Metallic Carbon Nanotubes by Gas-Phase Reaction. *Science* **2006**, *314*, 974–977.

31. Liu, B. L.; Jiang, H.; Krasheninnikov, A. V.; Nasibulin, A. G.; Ren, W. C.; Liu, C.; Kauppinen, E. I.; Cheng, H. M. Chirality-Dependent Reactivity of Individual Single-Walled Carbon Nanotubes. *Small* **2013**, *9*, 1379–1386.

32. Li, J. H.; Liu, K. H.; Liang, S. B.; Zhou, W. W.; Pierce, M.; Wang, F.; Peng, L. M.; Liu, J. Growth of High-Density-Aligned and Semiconducting-Enriched Single-Walled Carbon Nanotubes: Decoupling the Conflict between Density and Selectivity. *ACS Nano* **2014**, *8*, 554–562.

33. Cheung, C. L.; Kurtz, A.; Park, H.; Lieber, C. M. Diameter-Controlled Synthesis of Carbon Nanotubes. *J. Phys. Chem. B* **2002**, *106*, 2429–2433.

34. Li, Y.; Liu, J.; Wang, Y. Q.; Wang, Z. L. Preparation of Monodispersed Fe-Mo Nanoparticles as the Catalyst for CVD Synthesis of Carbon Nanotubes. *Chem. Mater.* **2001**, *13*, 1008–1014.

35. Baliyan, A.; Fukuda, T.; Uchida, T.; Nakajima, Y.; Hanajiri, T.; Maekawa, T. Synthesis of Diameter Controlled Carbon Nanotubes Using Self-Assembled Catalyst Nanoparticles. *Chem. Phys. Lett.* **2012**, *519*, 78–82.

36. An, L.; Owens, J. M.; McNeil, L. E.; Liu, J. Synthesis of Nearly Uniform Single-Walled Carbon Nanotubes Using Identical Metal-Containing Molecular Nanoclusters as Catalysts. *J. Am. Chem. Soc.* **2002**, *124*, 13688–13689.

37. Kukovitsky, E. F.; L'vov, S. G.; Sainov, N. A. VLS-Growth of Carbon Nanotubes from the Vapor. *Chem. Phys. Lett.* **2000**, *317*, 65–70.

38. Hasegawa, K.; Noda, S. Moderating Carbon Supply and Suppressing Ostwald Ripening of Catalyst Particles to Produce 4.5-mm-Tall Single-Walled Carbon Nanotube Forests. *Carbon* **2011**, *49*, 4497–4504.

39. Yang, F.; Wang, X.; Zhang, D. Q.; Yang, J.; Luo, D.; Xu, Z. W.; Wei, J. K.; Wang, J. Q.; Xu, Z.; Peng, F.; *et al.* Chirality-Specific Growth of Single-Walled Carbon Nanotubes on Solid Alloy Catalysts. *Nature* **2014**, *510*, 522–524.

40. Liu, K. H.; Hong, X. P.; Zhou, Q.; Jin, C. H.; Li, J. H.; Zhou, W. W.; Liu, J.; Wang, E. G.; Zettl, A.; Wang, F. High-Throughput Optical Imaging and Spectroscopy of Individual Carbon Nanotubes in Devices. *Nat. Nanotechnol.* **2013**, *8*, 917–922.

41. Ding, L.; Yuan, D. N.; Liu, J. Growth of High-Density Parallel Arrays of Long Single-Walled Carbon Nanotubes on Quartz Substrates. *J. Am. Chem. Soc.* **2008**, *130*, 5428–5429.

42. Dresselhaus, M. S.; Dresselhaus, G.; Saito, R. Carbon-Fibers Based on C-60 and Their Symmetry. *Phys. Rev. B* **1992**, *45*, 6234–6242.

43. Astakhova, T. Y.; Vinogradov, G. A.; Gurin, O. D.; Menon, M. Effect of Local Strain on the Reactivity of Carbon Nanotubes. *Russ. Chem. Bull.* **2002**, *51*, 764–769.

44. Srivastava, D.; Brenner, D. W.; Schall, J. D.; Ausman, K. D.; Yu, M. F.; Ruoff, R. S. Predictions of Enhanced Chemical Reactivity at Regions of Local Conformational Strain on Carbon Nanotubes: Kinky Chemistry. *J. Phys. Chem. B* **1999**, *103*, 4330–4337.

45. Godin, B.; Chen, Y. G.; Vaissermann, J.; Ruhlmann, L.; Verdaguer, M.; Gouzerh, P. Coordination Chemistry of the Hexavacant Tungstophosphate $[H_2P_2W_{12}O_{48}]^{12-}$ with Fe^{III} Ions: Towards Original Structures of Increasing Size and Complexity. *Angew. Chem., Int. Ed.* **2005**, *44*, 3072–3075.

46. Mbomekalle, I. M.; Lu, Y. W.; Keita, B.; Nadjo, L. Simple, High Yield and Reagent-Saving Synthesis of Pure α-$K_6P_2W_{18}O_{62} \cdot 14H_2O$. *Inorg. Chem. Commun.* **2004**, *7*, 86–90.